CORE PHYSICS VALIDATION FOR THE COMBUSTION ENGINEERING PWR

A. JONSSON
P. H. GAVIN
J. R. REC
W. B. TERNEY
Nuclear Engineering

Nuclear Power Systems
Combustion Engineering, Inc.
Windsor Connecticut

Presented by invitation at the
AMERICAN NUCLEAR SOCIETY WINTER MEETING
November 12-16, 1979
San Francisco, California

CE POWER SYSTEMS

CORE PHYSICS VALIDATION FOR THE COMBUSTION ENGINEERING PWR

I. INTRODUCTION

The Combustion Engineering, (C-E), core physics design relies on the following elements:

i) Generation of burnup dependent few-group spectrum averaged microscopic cross-section data (table sets) for use in coarse mesh and fine mesh, core-wide 2- and 3-dimensional depletion calculations, (DIT[1] and CEPAK[2,3,4] codes).

ii) Fine mesh (1x1 mesh per fuel pin) diffusion theory depletion calculations for selected axial elevations in the core, (2-D PDQ[5]).

iii) Coarse mesh (2x2 meshes per fuel assembly) higher order diffusion theory depletion calculations for the entire core in three dimensions, (3-D ROCS[6-11]).

The primary products of these elements are:

1) Reactivity and fuel lifetime predictions.
2) Reactivity coefficients for safety analyses.
3) Control rod worths.
4) Power distribution, isotopic content and burnup predictions.
5) Coefficient libraries for the in-core instrumentation.

Verification of the calculative tools has been continually carried out as they have evolved over the past 10 years. Use has been made of both basic critical experiments (to verify detailed reaction rates, reactivity and local power distribution) and of data from operating cores. C-E operating cores are being followed with 3-D simulations of the operation as they deplete for the triple purpose of verification of design, verification of design methods and verification of in-core instrument coefficient libraries. Recently, as more data from operating plants have become available, systematic trends have become apparent. This paper discusses the inter-related verification aspects of reactivity rundown accuracy and power distribution accuracy.

In Section II, reactivity trends are discussed for reload cores. Observed calculative reactivity errors are related to the choice of methods for generation of few-group cross-section data their impact on predicted power distributions is estimated in Section III. Actual power distribution performance of traditional and improved methods for generating few-group cross-section table sets is examined in Section IV.

II. REACTIVITY TRENDS IN RELOAD CYCLES

As a result of core follow programs carried out at C-E, a complete data base is in existence for cores with C-E fuel. This data base rests on the use of consistent methods through all past cycles, i.e.,ROCS/CEPAK utilizing a modified ENDF/B-IV library. The ROCS 3-D core simulator has been used in a 2-group version [11]. CEPAK combines a point model epithermally with a 1-dimensional, cylindrical pin cell model in the thermal energy region. The point model represents a volume weighted homogenization of an entire fuel assembly. The slowing down equations are solved in the B1 approximation as described in Ref. 2. Resonance cross-sections for U-238 are normalized to a combination of measured data from integral[12] and critical[13] experiments. Dancoff corrections are calculated to account for non-uniform shielding effects within each assembly type. The 1-dimensional, thermal model is based on THERMOS[3] modified to use improved integral transport matrices[14]. Non-fuel components of the assembly such as water holes, burnable absorbers and control rods are treated by separate, 1-dimensional, cylindrical transport calculations in the thermal range. Simplified representations are employed to represent the environment within the 1-dimensional geometry.

The calculative model described yields the reactivity agreement shown in Figure 1 for reload cycles. In general, one observes relatively good agreement at BOC and maximum reactivity differences of the order of 1%$\Delta\rho$ between the predictions and the measurements at each EOC. The pattern repeats itself with considerable consistency.

This fact facilitates the process of biasing cycle length predictions and core reactivity data. The feature that is of interest in this paper is the steady trend with core average burnup. Figure 1 shows that the calculations steadily lose reactivity faster than the cores do in operation. The difference in rate of reactivity loss is about 0.5%$\Delta\rho$ per 10,000 MWD/T. Consistent reactivity errors are observed when using the CEPAK cross-section data base in fine mesh PDQ core depletions. This confirms the accuracy of the coarse mesh simulator, ROCS, and indicates that the source of the trend is connected with the few-group cross-section data (whether for fine mesh or coarse mesh) generated as described above. As will be shown below, Section III, this trend in the reactivity error is of concern because of the coupling between local reactivity error and global power distributions in PWR cores.

III. METHODS-RELATED UNCERTAINTIES IN REACTIVITY AND THEIR IMPACT ON POWER DISTRIBUTIONS

The development of the DIT code[1] was initiated in 1973[15,16] for the purpose of improving reactivity predictive capability as well as for dealing with the related problems of generating assembly average few-group cross-sections for coarse mesh table sets.

Essential differences between DIT and traditional few-group cross-section generation methods are as follows:

1) The neutron energy spectrum is calculated with detailed attention to the actual assembly geometry both epithermally and thermally. Spectrum interactions between fuel, absorbers and water holes are therefore accounted for more accurately than is possible with traditional methods.

2) The calculation of space dependent spectra is followed by a few group, transport theory calculation in the actual assembly geometry (pins are not homogenized) the purpose of which is to provide coarse mesh averaged cross-sections consistent with the fine mesh, few-group cross sections that are generated within the same run. This transport calculation permits more accurate estimates of local flux peaking and dipping than provided by traditional methods that rely on combinations of 1-dimensional transport calculations and diffusion theory.

3) The use of improved cross-section representations and basic data in the resonance region.

Figure 2 shows the physics contents of the DIT code and the way it links to PDQ and ROCS. The Figure also shows the linkages with ENDF/B-IV. All conclusions in this paper are based on the use of ENDF/B-IV including modifications of fission spectra and of U-238 resonance absorption as described by Jonsson, et al[1].

Methods related improvements for the reactivity rundown shape have been achieved both in simple uniform lattice fuel geometry and in the non-uniform assembly geometries of the PWR. Figure 3 shows reactivity differences as a function of fuel depletion. These differences are between improved (DIT) and traditional (CEPAK) methods applied to a simple uniform lattice of 3 w/o fuel. Also shown is the difference between WIMS D4[17,18] and CEPAK. In all three codes, the depletion of this uniform lattice was followed by a soluble boron rundown to essentially zero ppm concentration in each of three cycles. A cycle dependent but otherwise constant buckling was used to account for the influence of leakage on the spectrum. Although detailed differences exist between DIT and WIMS, one can see that they both predict a more positive reactivity trend within each cycle than the traditional methods represented by CEPAK. This difference has been traced to differences in k_∞ (resonance absorption and slowing down power, but little contribution from fission products). It is a major contribution to reactivity rundown errors observed with traditional methods for reload cores. Figure 3 also shows that there is a difference in the prediction of the change in leakage that takes place at each cycle change in this particular calculation. This difference is of little significance for full core reactivity rundown where the leakage is relatively small.

Figure 4 shows a similar comparison between improved and traditional methods for an assembly geometry with 16x16 fuel and water filled control rod locations. The trend of a less rapid reactivity depletion prediction by improved methods is observed also in this geometry. The trend has been found to be enrichment dependent. In assembly geometry various spectrum interaction phenomena contribute to the net reactivity difference seen between improved and traditional methods. Table 1 (thermal energies) and Table 2 (epithermal energies) list, for fresh fuel, the reactivity worths of some of the interaction effects. It can be seen that the slowing down cross-section is particularly important. In general, one finds an increase of group removal cross-sections for fuel cells adjacent to water holes. These effects are typically of the order of 3.5 to 4% and are due to a shift to lower energies in the spectrum in the range 2eV to 5keV. The net reactivity effect in a PWR assembly with about 20 water holes is around 0.5 to 0.6%k. It is always counteracted by an increase of the local value of the Dancoff factor worth typically some -0.3%k.

TABLE 1

NON-UNIFORM LATTICES. EFFECTS OF THERMAL SPECTRUM INTERACTIONS ON REACTIVITY

Fuel Type	Temperature	Physical Effect	Effect on Reactivity
UO_2	Operating	Hardening of spectrum for fuel close to absorbers.	-0.10 to -0.15%k
UO_2	Operating	Softening of spectrum for fuel close to waterholes.	
		a) Effect due to change in σ_a	-0.65%k
		b) Effect due to change in $\nu\sigma_f$	+0.70%k
		c) Net effect	+0.05%k
UO_2	Cold condition	As above, net effect	+0.20 - 0.25%k
Mixed oxide	Operating	As above, net effect	+0.70%k
Mixed oxide	Cold condition	As above, net effect	+0.25%k
UO_2	Operating	Softening of spectrum in burnable absorber relative to simple 1-D method.	-0.15 to -0.30%k

TABLE 2

NON-UNIFORM LATTICES. EFFECTS OF EPITHERMAL SPECTRUM INTERACTIONS ON REACTIVITY 1)

Fuel Type	Physical Effect	Effect on Reactivity
UO_2	Softening of Resonance region spectrum for fuel near waterholes.	
Without burnable absorbers.	Effect on slowing down.	+0.55%k
With burnable absorbers	Effect on slowing down.	+0.10%k
Without burnable absorbers.	Effect on resonance absorption	-0.30%k
With burnable absorbers	Effect on resonance absorption.	-0.15 to -0.20%k

1) Relative to conditions for infinite lattice.

The difference observed between improved and traditional methods in Figures 3 and 4 are substantial. The use of DIT therefore permits a more accurate determination of cycle end points. This fact is not of overriding importance, however, since reactivity life time is a quantity which is easily "calibrated" given enough of operating data. The impact of reactivity errors on the global power distribution is not so easily predicted, however, unless these errors have been minimized by the calculative method. Figures 5, 6 and 7 show the predicted power distribution effects of removing a systematic reactivity error of 0.4-0.5%$\Delta\rho$ per 10,000 MWD/T of local burnup. These predictions were made by applying a reactivity perturbation to the k_∞ distribution in

a nodal simulator[13]. Although using batch independent reactivity perturbation on k_∞ and other simplifications, this survey provided initial understanding of the phenomena involved in the interaction between local burnup dependent reactivity error and global power distribution. The same pattern repeats itself at each BOC: Fig. 5 (BOC 2), Fig. 6 (BOC 3) and Fig. 7 (BOC 4). It is seen that removing the reactivity bias would raise the predicted power in the center of the core (predominatly old fuel) and lower it on the edge of the core (new fuel). The size of this in/out power swing depends on the details of how the fuel management mixes old and new fuel. On the basis of survey calculations of this nature, it was determined that the size of the power roll would be of the order of 0.04 to 0.08 relative power density units. This represents the estimated calculative uncertainty originating from methods uncertainties in the reactivity rundown. Because of the nature of the interaction between local reactivity, global power and local burnup, this uncertainty is largest at the beginning of each cycle. As the power error generally results in a compensating error in local burnup, the error decreases throughout each cycle. For long fuel cycles with larger contrast between the reactivities of fresh and depleted fuel, the effects at BOC may be larger than has been illustrated here for cycle lengths of 9-10,000 MWD/T.

IV. POWER DISTRIBUTIONS FOR RELOAD CYCLES

In this section, comparisons are presented between the results of traditional and improved methods and measurements of the power distribution in reload cycles.

Traditional Methods

Figure 8 shows how cross section table sets based on traditional methods perform well in first cycles starting with fresh fuel. This is a consequence of the good initial reactivity performance of these methods and of the fact that reactivity error induced power distribution perturbations tend to be compensated by the associated burnup error. The figure shows the power distribution at the mid-core level near BOC 1. The maximum positive error in relative box power is 0.015 (absolute units) and the standard deviation between calculation and measurement is only 0.009 or approximately 1%.

As noted in the previous section, the calculative power distribution error is expected to burn down. Figure 9 shows a second cycle at about 5000 MWD/T through the cycle. No systematic trends can be observed here. The maximum error between calculation and measurement is 0.022 relative box power units and the standard deviation is still about 1%.

For first cycles and for advanced burnups in later cycles the agreement is thus observed to be good. The following three figures, Fig. 10 for BOC 2, Fig. 11 for a BOC 3 and Fig. 12 for a BOC 4 show a different picture however.

The measured radial power distributions are consistently more peaked to the center of the core than the calculations. The differences illustrated are for the axial mid-regions of the core and 500-1000 MWD/T into each cycle. Underpredictions of power in the central assemblies are typically 0.03 to 0.07 for the relative box power. Furthermore, the radial distribution of the observed error is in close proximity of the estimates described in Section III. It was therefore seen that the differences between measurements and calculations are consistent with the presence of the reactivity error shown in Figure 1.

Improved Methods

The DIT code described in Section III and in Ref. 1 has been in use for analysis of operating cores since 1976 and a base is now available that is large enough to permit general trends to be visible.

Figure 13 shows the reactivity rundown agreement for all but one of the cores included in Figure 1. For reload cycles an essentially constant and small reactivity bias of about -0.2%$\Delta\rho$ is observed. The fact that it is constant is significant since it implies that the reactivity of depleted fuel is predicted with the same accuracy as fresh fuel. This minimizes box power errors in the early portions of reload cycles and leads to global power distributions in better agreement with the true power distribution. For first cycles, the use of DIT-based cross-section table sets improves reactivity but does not lead to appreciable changes in the good power distribution performance observed for traditional methods. This is illustrated by Fig. 14 from a recent plant startup. The axially integrated power distribution is shown in a comparison between 3-D ROCS (DIT) and the measured power distribution as determined by the full-core instrumentation system CECOR[20]. The maximum deviation observed is -0.02 (at the center of the core) and the standard deviation is 0.009 relative box power units or approximately 1%.

Figures 15 and 16 show ROCS (DIT) versus CECOR comparisons for the early portions of reload cycles, Fig. 15 for cycle 3 and Fig. 16 for a cycle 4. Radial distributions for the axial mid-regions of the core are shown. A certain degree of overcompensation has been observed in some cases in the sense that the use of cross-section table sets based on DIT tend to overpredict power in old fuel when located in the central regions of the core. In other cases, such as the cycle 4 results of Figure 16, a small underprediction is still noticed. The major effect of employing improved table sets has, however, been to correct the radial shift in the calculated power distribution observed with traditional methods.

V. SUMMARY AND CONCLUSIONS

The consistently observed reactivity loss of traditional cross-section table sets relative to data from operating plants has been corrected by the development of improved methods for calculating few-group fine mesh and coarse mesh table sets. The improvements in reactivity rundown accuracy have led to an important reduction of the level of the calculative uncertainty for power distributions in reload cycles. Systematic in/out radial shifts, relative to measured power distributions, resulting in maximum calculative errors in assembly power of typically 10%, have been eliminated.

The driving mechanism for the observed radial power distribution shifts is the burnup dependent reactivity bias which creates an error in the calculated reactivity difference between old and new fuel. Physics effects reflected in the differences between traditional and improved methods have been identified. They originate both in the epithermal and thermal neutron energy region. A major portion of the improvement is connected with the treatment of resonance absorption and its resulting effects on slowing down power. This portion appears even in the simple geometry of a uniform fuel pin lattice. Other contributions to the improvement are related to the non-uniform nature of the PWR fuel assembly. They emanate from the details of the spectrum interactions between water holes and fuel or between burnable absorbers and fuel. In the epithermal region, for example, traditional methods afford a too simplified picture of spectrum interactions which often result in an underprediction of the removal cross sections for water holes and adjacent fuel. This affects both reactivity and thermal events such as local flux peaking.

In conclusion, it has been found advantageous to employ a table set generation procedure which is based on fundamental data and methods and which avoids more or less arbitrary adjustments of cross-sections. In this way significant improvements in the accuracy of reactivity lifetime and core power distribution have been achieved that simultaneously maintain or improve the accuracy in other areas such as local peaking[1] and reactivity coefficients.

REFERENCES

1. A. Jonsson, J. R. Rec, U. N. Singh, "Verification of a Fuel Assembly Spectrum Code Based on Integral Transport Theory," Trans. Am. Nucl. Soc. 28, 778 (1978).

2. D. McGoff, 'FORM - A Fourier Transform Fast Spectrum Code for the IBM 709," NAA-SR-Memo 5766, 1960.

3. H. C. Honeck, "THERMOS, A Thermalization Transport Theory Code for Reactor Lattice Calculations," BNL 5826, 1962.

4. T. R. England, "Time Dependent Fission Product Thermal and Resonance Absorption Cross Sections," WAPD-TM-333, 1962.

5. W. R. Cadwell, "PDQ-7 Reference Manual," WAPD-TM-678, 1967.

6. C. P. Robinson, J. D. Eckard, Jr., "A Higher Order Difference Method for Diffusion Theory," Trans. Am. Nucl. Soc., 15, 297 (1972).

7. C. P. Robinson and R. R. Lee, "Experimental Verification of the 3-D Coarse Mesh Method of Robinson and Eckard," Trans. Am. Nucl. Soc., 17, 476 (1973).

8. I. C. Rickard, N. R. Gomm, T. G. Ober, "Calculational and Experimental Verification of the Combustion Engineering Coarse Mesh Physics Simulator," Trans. Am. Soc., 24, 340 (1976).

9. T. G. Ober, J. C. Stork, I. C. Rickard, J. K. Gasper, "Theory, Capabilities, and Use of the Three-Dimensional Reactor Operation and Control Simulator (ROCS)," Nucl. Sci. Eng., 54, 605, (1977).

10. T. G. Ober, J. C. Stork, R. P. Bandera, W. B. Terney, "Extension of the ROCS Coarse Mesh Physics Simulator to Two Energy Groups," Trans. Am. Nucl. Soc., 28 , 763 (1978).

11. W. B. Terney, R. P. Bandera, T. G. Ober, "Qualification of C-E's 3-D Spatial Neutronics Code for PWR Analysis," Trans. Am. Nucl. Soc., 30, 227 (1978).

12. E. Hellstrand, "Measurement of Resonance Integrals," ANS Topical Meeting, San Diego, 1966. P. 151 of proceedings edited by A. J. Goodjohn and G. C. Pomraning, The M.I.T. Press, 1966.

13. P. B. Kemshell, "Some Integral Properties of Nuclear Data Deduced from WIMS Analyses of Well Thermalized Uranium Lattices," AEEW-R786, (1972).

14. I. Carlvik, "Integral Transport Theory in One-dimensional Geometries," Nukleonik, 10, 104, (1967).

15. A. Jonsson, et.al., "Discrete Integral Transport Theory Extended to the Case with Surface Sources," Atomkernenergie, 24, 79-84, (1974).

16. A. Jonsson, et.al., "Integral Transport Theory with Cell Couplings Involving Arbitrarily Distributed Currents," Trans. Am. Nucl. Soc., 21, 231, (1975).

17. J. R. Askew, et.al., "A General Description of the Lattice Code WIMS," Journal Brit. Nucl. Energy Soc., 5,4, (1966).

18. M. J. Halsall, personal communication.

19. W. B. Terney, E. A. Williamson,Jr., "The Design of Reload Cores Using Optimal Control Theory," Trans. Am. Nucl. Soc., Vol.27, p. 361, (1977).

20. W. B. Terney, E. A. Williamson, Jr., T. G. Ober, "Calculational Verification of C-E's New Full-core Instrumentation System," Trans. Am. Nucl. Soc., Vol. 24, P. 429, (1976).

FIGURE 1

LATER CYCLE REACTIVITY ERRORS, CONVENTIONAL METHODS

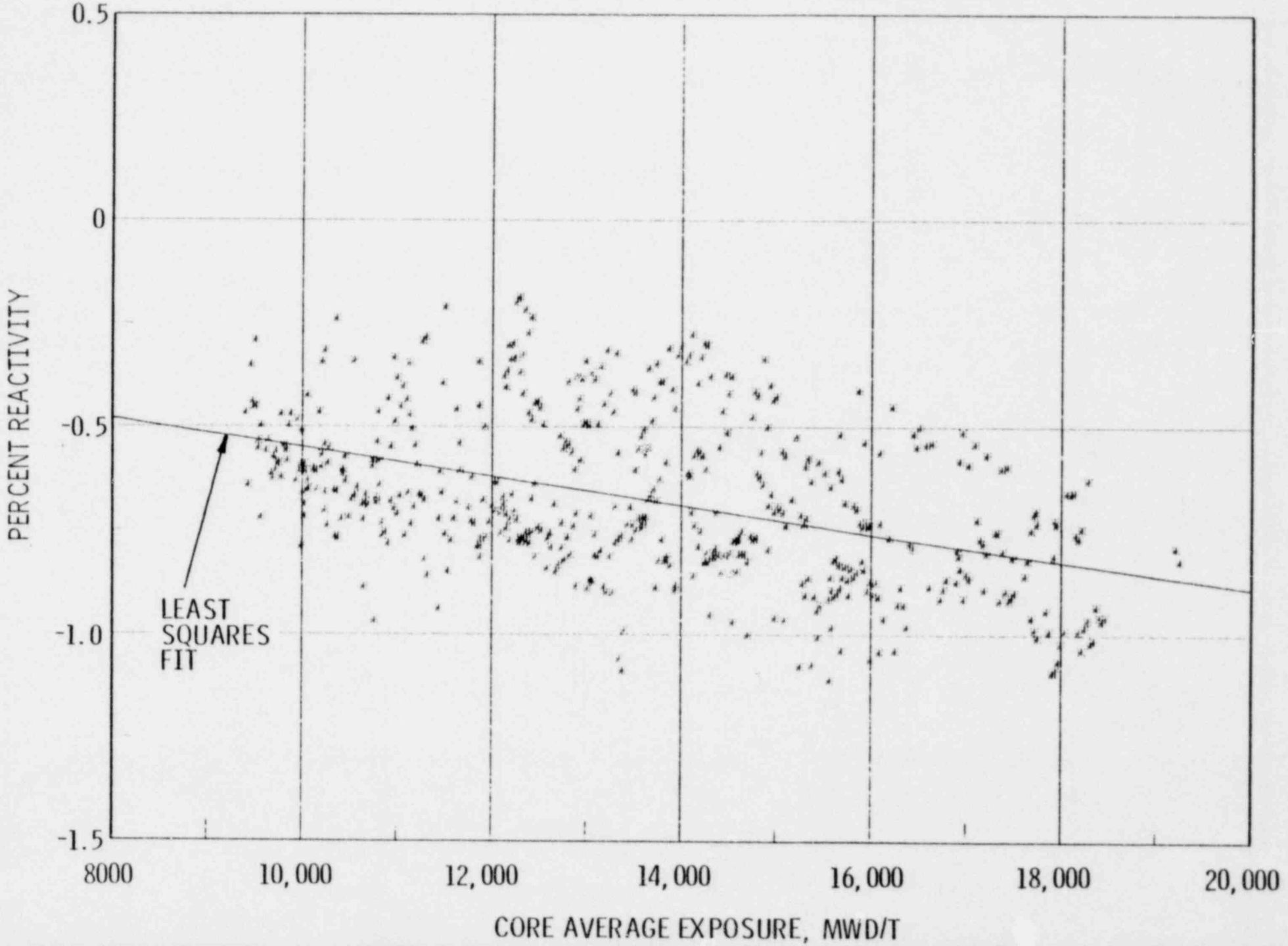

Figure 2

THE DIT ASSEMBLY CODE

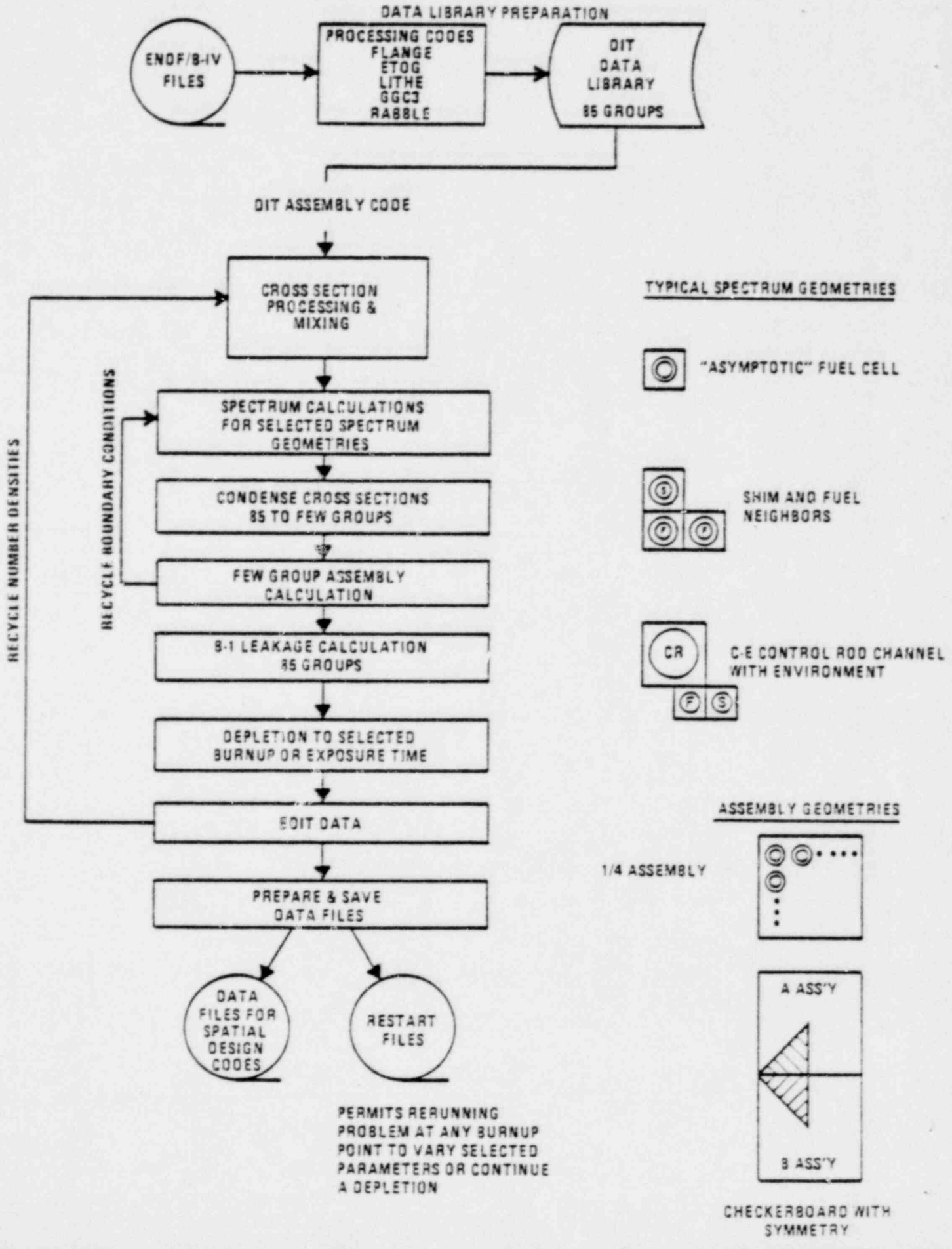

Figure 3

REACTIVITY DIFFERENCE BETWEEN IMPROVED AND TRADITIONAL CROSS SECTION GENERATION METHODS: 3 W/O PIN CELL

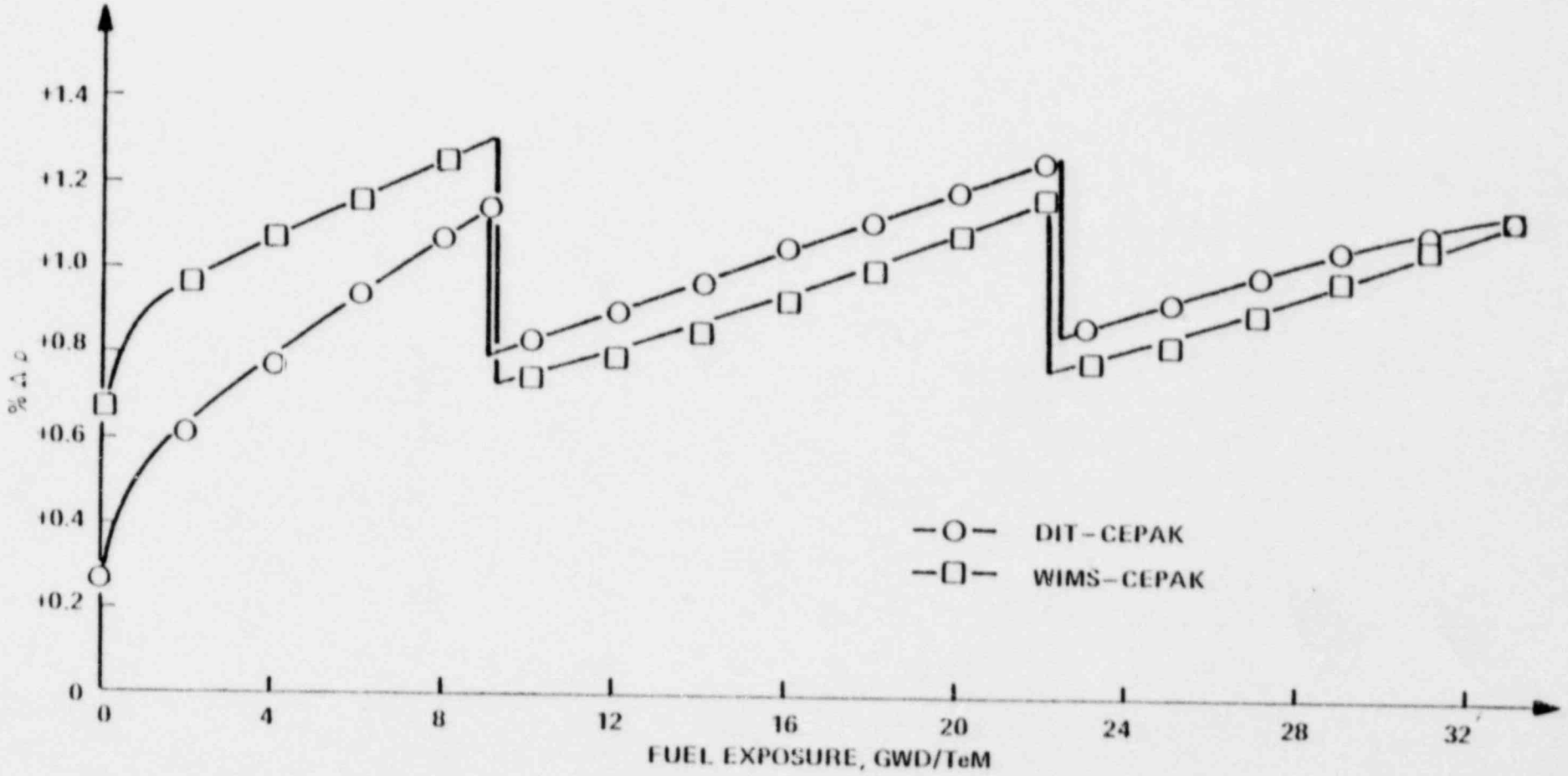

Figure 4

REACTIVITY DIFFERENCE BETWEEN IMPROVED AND TRADITIONAL CROSS SECTION GENERATION METHODS: 3 W/O ASSEMBLY

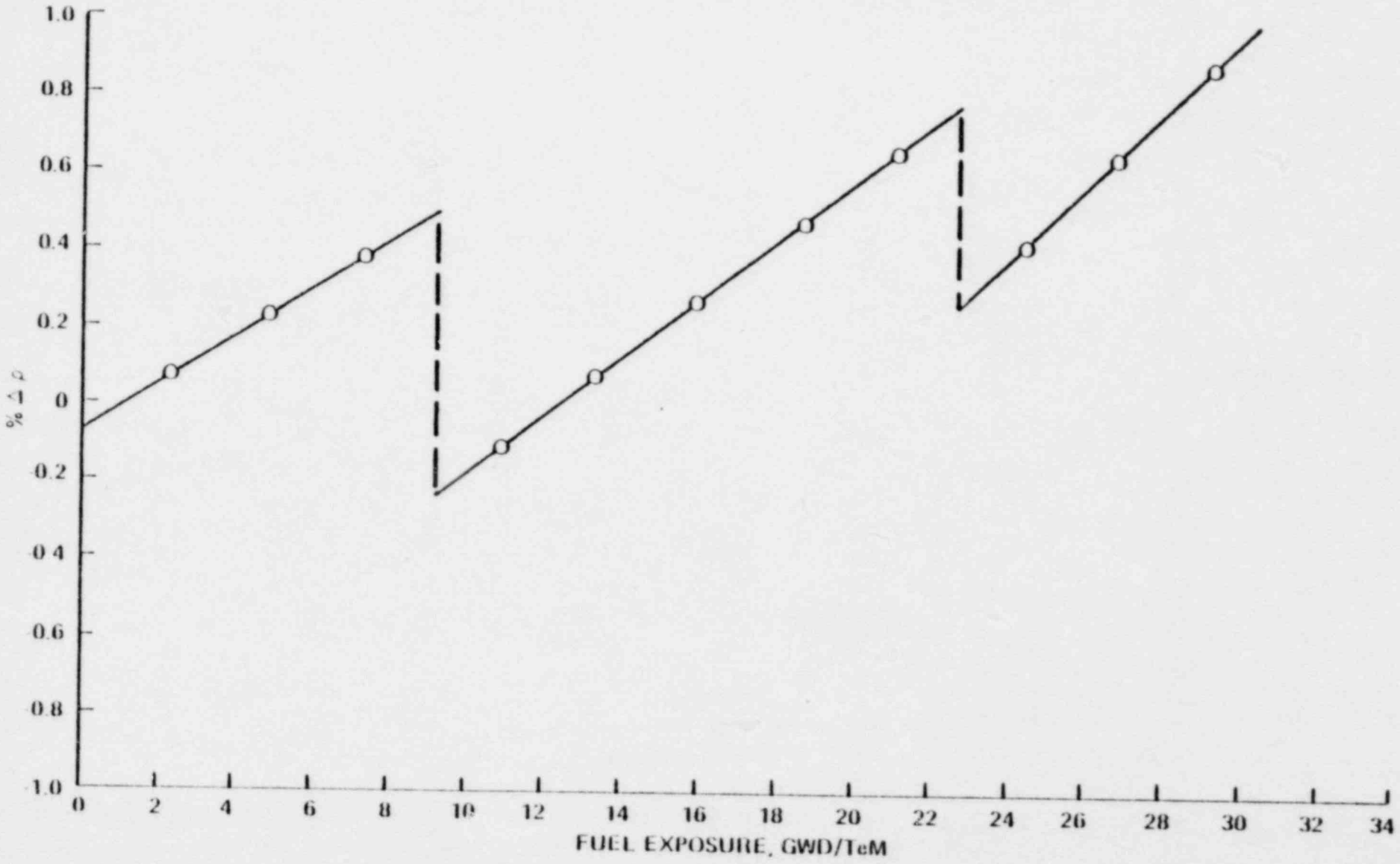

Figure 5

PREDICTED EFFECT OF REMOVING REACTIVITY BIAS ON POWER DISTRIBUTIONS, BOC 2

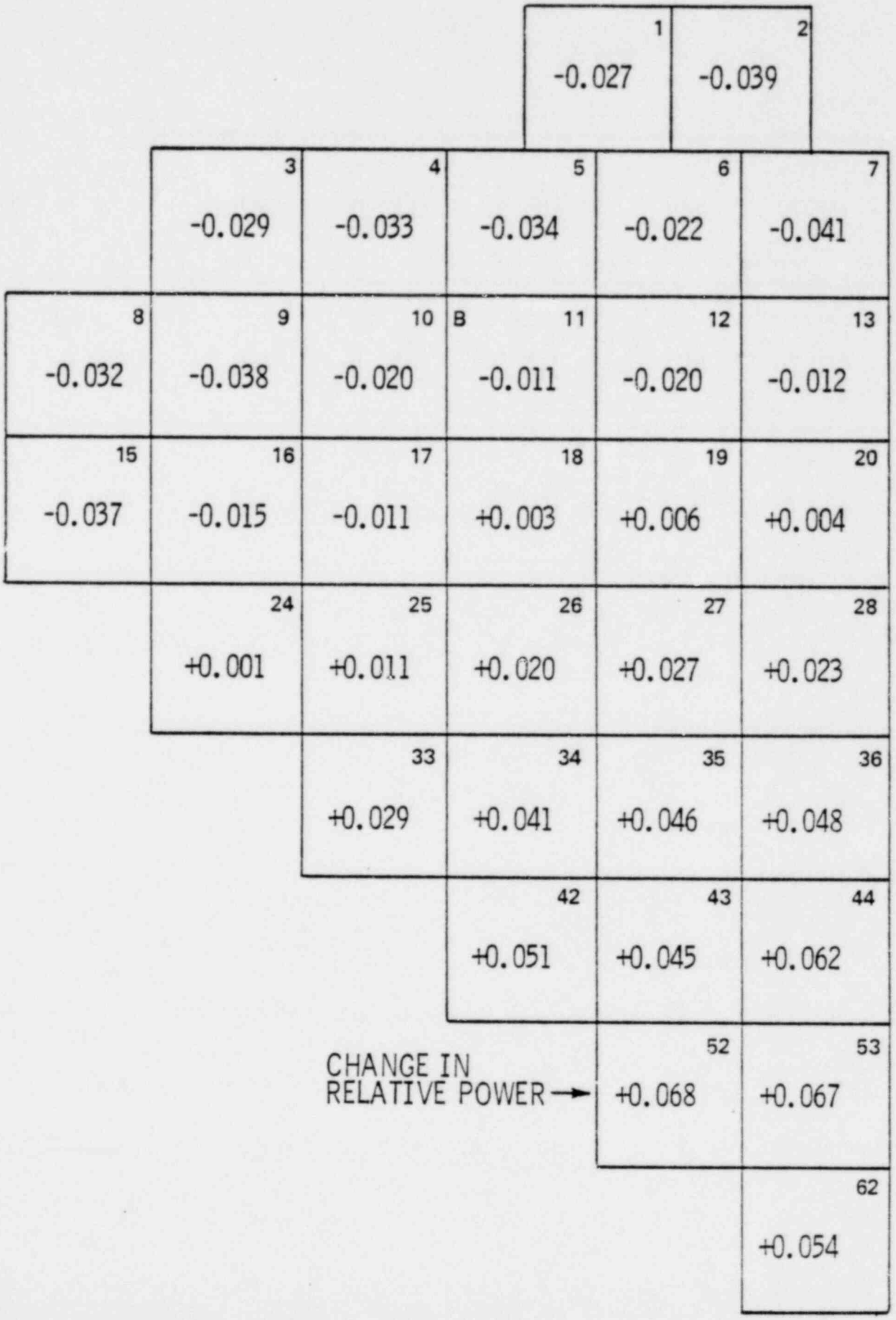

Figure 6

PREDICTED EFFECT OF REMOVING REACTIVITY BIAS ON POWER DISTRIBUTIONS, BOC 3

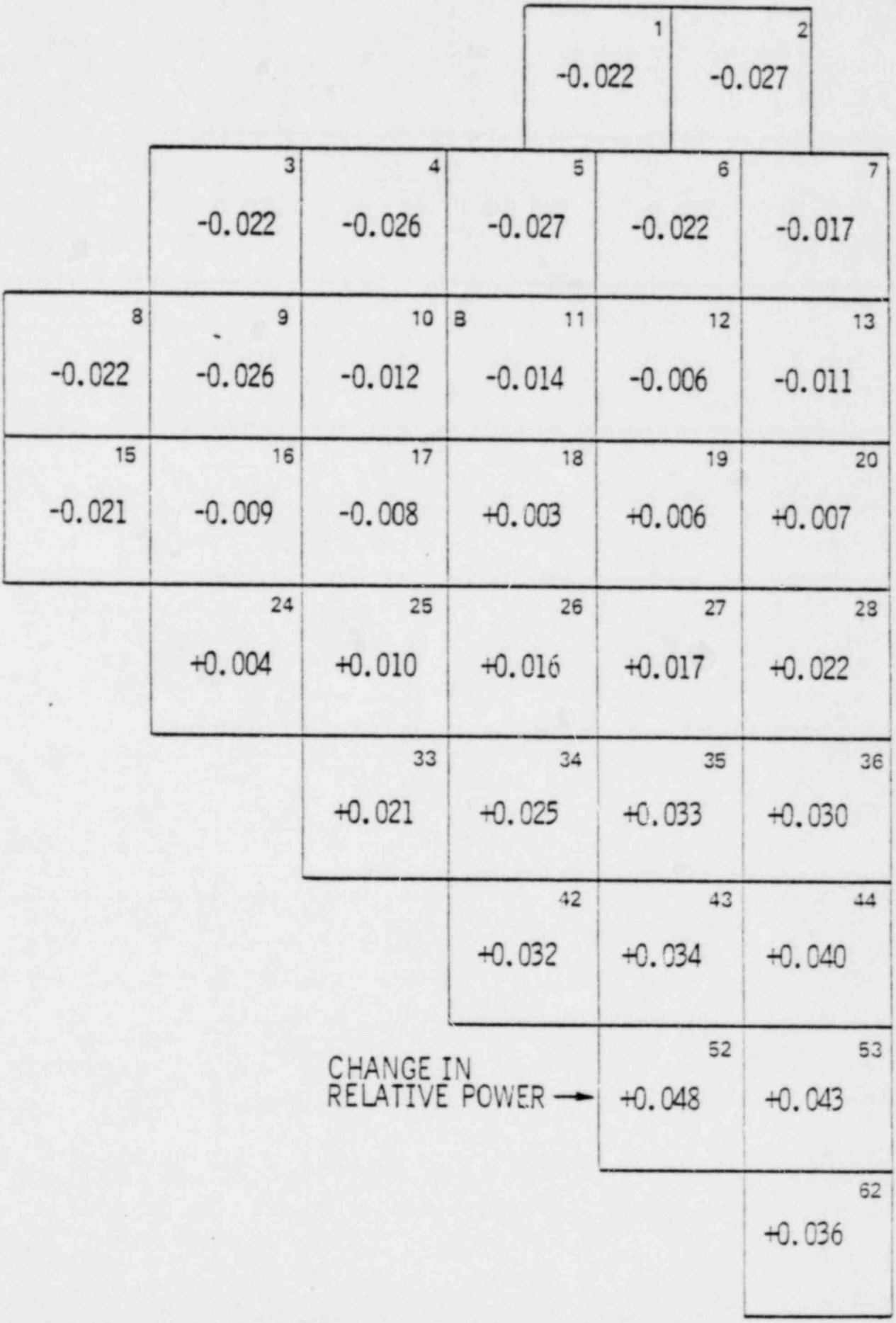

Figure 7

PREDICTED EFFECT OF REMOVING REACTIVITY BIAS ON POWER DISTRIBUTIONS, BOC 4

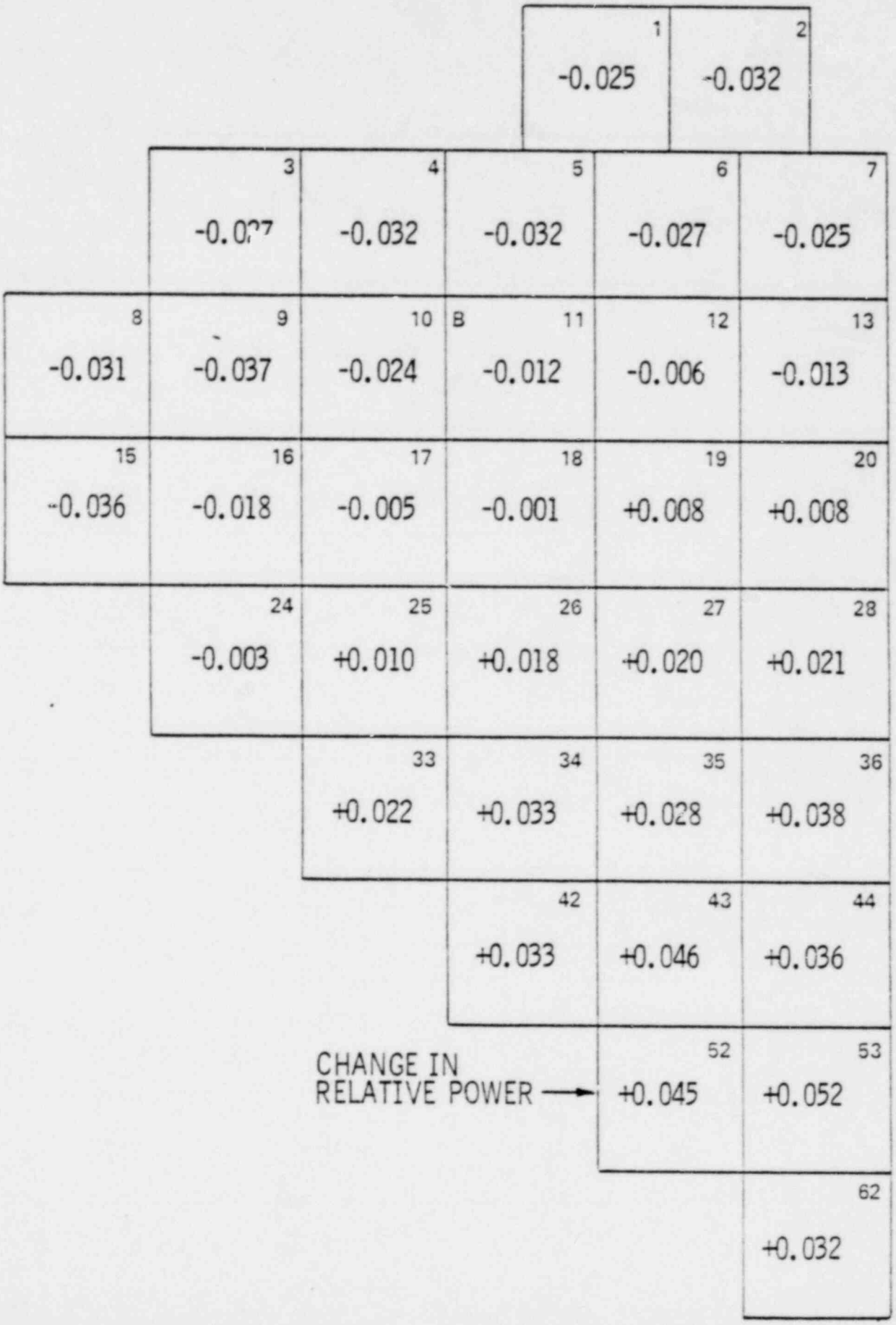

Figure 8

CALCULATED AND MEASURED POWER DISTRIBUTIONS, BOC 1
(TRADITIONAL METHODS)
BOC 1 LEVELS 2 - 3

MEAS C - M						
					0.600 0.000	0.780 -0.001
		0.568 0.013	0.781 0.009	0.960 -0.003	1.115 -0.022	0.989 -0.012
	0.667 0.006	1.010 0.001	0.958 0.012	1.024 0.010	1.067 -0.009	1.058 0.000
0.667 0.006	1.055 -0.006	1.012 -0.002	1.036 0.011	1.085 -0.006	1.085 0.005	1.113 -0.013
0.573 0.007	1.011 -0.001	1.014 -0.005	1.051 0.006	1.097 -0.007	1.095 0.008	1.125 -0.009	1.109 0.005
0.781 0.009	0.955 0.015	1.035 0.011	1.098 -0.008	1.098 0.006	1.132 -0.009	1.113 0.012	1.145 -0.012
0.957 -0.000	1.022 0.012	1.083 -0.004	1.096 0.007	1.136 -0.012	1.123 0.005	1.148 -0.008	1.131 0.005
0.599 0.000							
1.114 -0.021	1.068 -0.010	1.085 0.005	1.126 -0.010	1.117 0.008	1.153 -0.012	1.135 0.004	1.160 -0.012
0.778 0.001							
0.989 -0.012	1.058 0.000	1.113 -0.013	1.109 0.005	1.145 -0.012	1.131 0.005	1.160 -0.012	1.140 0.003

Figure 9

CALCULATED AND MEASURED POWER DISTRIBUTIONS, MOC 2
(TRADITIONAL METHODS)

MEAS C - M							
					0.676 0.010	0.902 0.016	
			0.719 0.022	0.934 0.018	1.064 0.006	0.910 0.006	1.246 −0.004
		0.841 0.011	1.161 0.012	1.044 0.008	0.910 0.000	1.241 −0.014	1.006 −0.002
	0.838 0.015	1.180 0.011	1.060 0.008	1.223 −0.012	0.900 −0.010	0.914 −0.010	1.244 −0.027
0.731 0.010	1.164 0.010	1.056 0.012	0.998 0.000	0.885 0.000	0.890 −0.011	1.003 −0.016	0.915 −0.010
0.940 0.013	1.047 0.005	1.219 −0.007	0.879 0.008	1.095 −0.016	1.128 −0.011	1.064 −0.014	1.057 −0.014
1.067 0.004	0.910 0.000	0.895 −0.004	0.888 −0.007	1.129 −0.012	1.117 −0.010	0.930 0.010	1.115 −0.006
0.675 0.011							
0.910 0.006	1.242 −0.015	0.913 −0.009	1.003 −0.016	1.066 −0.015	0.927 0.013	1.095 −0.003	1.069 0.003
0.898 0.020							
1.246 −0.004	1.006 −0.002	1.244 −0.026	0.915 −0.010	1.057 −0.013	1.115 −0.006	1.069 0.004	0.935 0.009

Figure 10

CALCULATED AND MEASURED POWER DISTRIBUTIONS, BOC 2
(TRADITIONAL METHODS)

MEAS C - M							
						0.635 0.024	0.872 0.035
			0.719 0.044	0.928 0.050	1.037 0.040	0.883 0.017	1.233 0.024
		0.871 0.040	1.207 0.053	1.060 0.027	0.882 0.012	1.217 0.009	0.989 0.000
	0.870 0.041	1.245 0.050	1.106 0.024	1.238 0.012	0.869 -0.011	0.880 -0.016	1.218 -0.018
0.730 0.034	1.212 0.048	1.104 0.027	1.004 0.010	0.873 -0.006	0.866 -0.026	0.983 -0.042	0.892 -0.032
0.936 0.042	1.068 0.020	1.236 0.015	0.869 0.000	1.107 -0.040	1.148 -0.045	1.078 -0.054	1.078 -0.064
1.044 0.034	0.884 0.010	0.860 -0.001	0.864 -0.022	1.152 -0.047	1.146 -0.053	0.942 -0.034	1.150 -0.063
0.632 0.028							
0.884 0.017	1.221 0.005	0.880 -0.014	0.983 -0.041	1.082 -0.058	0.936 -0.028	1.133 -0.062	1.111 -0.057
0.864 0.043							
1.233 0.024	0.989 0.000	1.218 -0.017	0.892 -0.031	1.078 -0.064	1.150 -0.062	1.111 -0.056	0.957 -0.042

Figure 11

CALCULATED AND MEASURED POWER DISTRIBUTIONS, BOC 3
(TRADITIONAL METHODS)

MEAS C - M							
						0.728 0.018	0.931 0.023
			0.682 0.032	0.932 0.040	1.114 0.039	1.107 0.011	0.980 0.005
		0.814 0.005	1.128 0.028	0.845 0.054	1.210 0.008	0.987 0.011	1.302 −0.009
	0.806 0.012	1.107 −0.001	0.963 0.007	1.266 0.007	0.974 0.004	1.186 −0.022	0.867 0.001
0.704 0.012	1.143 0.014	0.974 −0.003	0.881 −0.005	0.943 −0.003	1.052 −0.010	0.871 −0.003	1.176 −0.046
0.954 0.022	0.864 0.038	1.284 −0.004	0.947 −0.007	1.175 −0.023	0.948 −0.014	1.173 −0.037	0.998 −0.046
1.134 0.027	1.227 −0.000	0.981 0.003	1.059 −0.014	0.957 −0.019	0.880 −0.027	0.841 −0.017	1.000 −0.036
0.740 0.011							
1.118 0.010	0.995 0.013	1.193 −0.019	0.876 −0.001	1.181 −0.033	0.852 −0.018	1.087 −0.045	0.898 −0.037
0.940 0.021							
0.980 0.014	1.302 0.003	0.867 0.009	1.176 −0.035	0.998 −0.034	1.002 −0.025	0.898 −0.033	0.748 −0.022

Figure 12

CALCULATED AND MEASURED POWER DISTRIBUTIONS, BOC 4
(TRADITIONAL METHODS)

MEAS C - M							
						0.681 0.004	0.876 0.007
			0.724 0.019	0.986 0.023	1.115 0.020	1.102 -0.006	1.065 0.002
		0.835 0.012	1.207 0.022	1.201 0.017	1.011 0.010	0.895 -0.003	1.242 -0.021
	0.839 0.009	1.233 0.010	1.101 0.011	1.036 0.009	1.226 0.010	0.938 -0.014	0.967 -0.019
0.721 0.024	1.213 0.020	1.102 0.013	1.043 0.012	0.994 0.006	0.923 0.000	1.000 -0.011	0.878 -0.014
0.995 0.019	1.216 0.007	1.045 0.011	1.000 0.009	0.939 0.011	1.099 -0.017	0.829 -0.008	1.059 -0.036
1.130 0.011	1.023 0.006	1.245 0.004	0.929 0.004	1.099 -0.011	0.852 -0.008	1.082 -0.032	0.846 -0.020
0.691 -0.002							
1.109 -0.007	0.899 0.004	0.944 0.000	1.003 -0.006	0.826 -0.003	1.081 -0.030	0.989 -0.037	1.102 -0.063
0.880 0.008							
1.065 0.009	1.242 -0.007	0.967 -0.006	0.878 -0.007	1.059 -0.032	0.846 -0.020	1.102 -0.065	0.708 -0.050

FIGURE 13

LATER CYCLE REACTIVITY ERRORS, IMPROVED METHODS

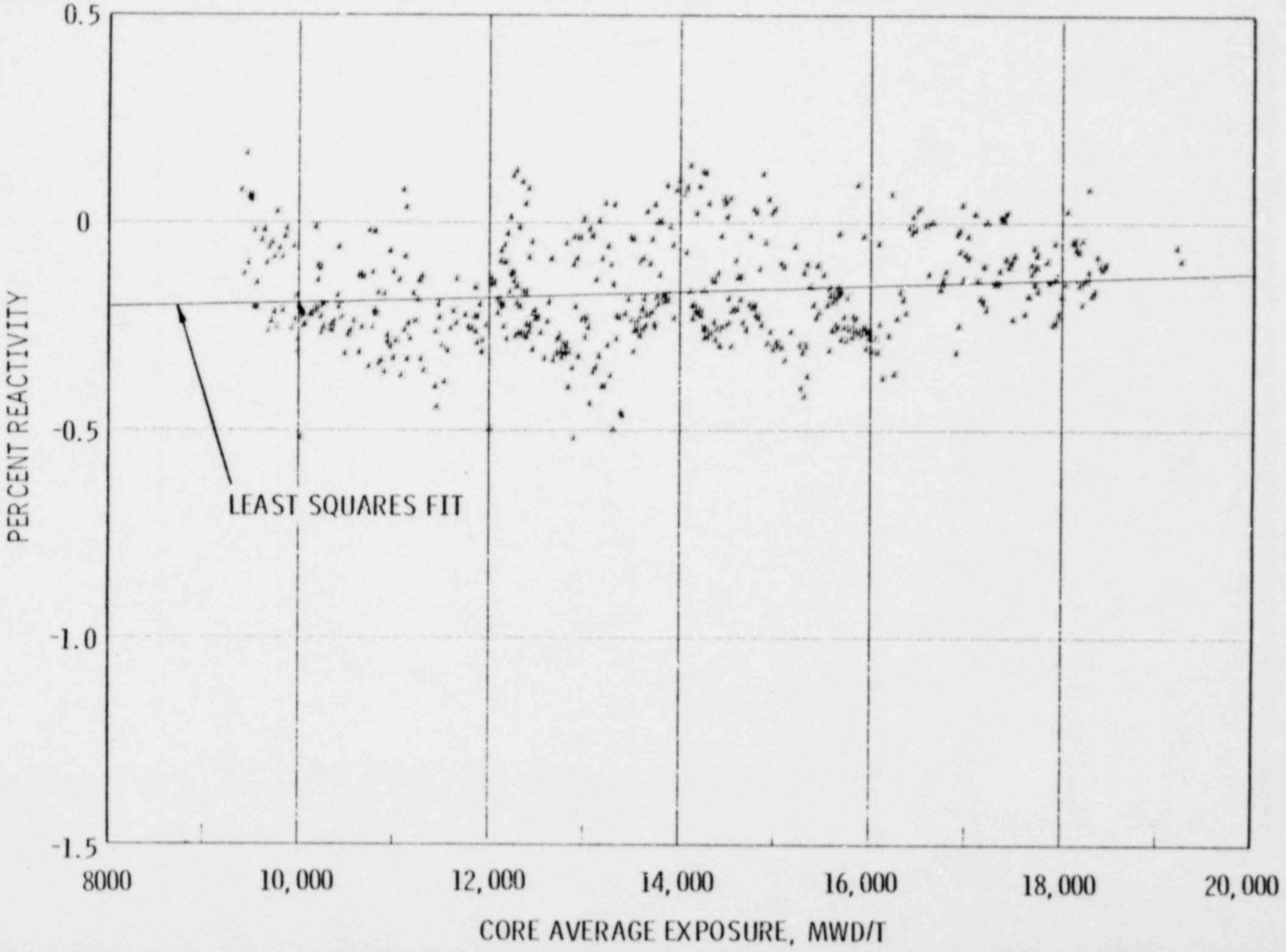

Figure 14

CALCULATED VERSUS MEASURED RELATIVE BOX POWER, BOC
(IMPROVED METHODS)

CALC - MEAS							
					0.019	0.015	0.011
			0.006	0.009	0.005	0.016	0.001
		0.010	-0.004	0.002	0.002	-0.004	-0.002
	0.009	0.002	0.002	-0.001	-0.008	-0.008	-0.011
	0.012	0.007	0.003	-0.006	-0.004	-0.010	-0.007
0.016	0.004	0.007	-0.006	-0.005	-0.010	-0.004	-0.014
0.012	0.006	-0.005	-0.007	-0.012	-0.009	-0.016	-0.017
0.011	0.001	-0.002	-0.011	-0.007	-0.014	-0.017	-0.021

Figure 15

CALCULATED AND MEASURED POWER DISTRIBUTIONS, BOC 3

(IMPROVED METHODS)

MEAS C - M							
					0.709 -0.016	0.871 -0.006	
			0.600 -0.009	0.881 -0.004	1.148 0.000	1.103 -0.004	0.904 0.008
		0.695 -0.028	0.927 -0.012	0.768 0.028	1.217 0.006	0.805 0.026	0.912 0.001
	0.696 -0.025	1.018 -0.026	0.779 -0.006	1.230 0.002	1.136 0.014	1.144 0.009	1.280 -0.001
0.622 -0.023	0.949 -0.025	0.781 -0.004	1.205 -0.022	0.831 0.022	1.022 0.009	1.226 0.011	1.080 0.010
0.912 -0.024	0.812 0.002	1.252 -0.011	0.833 0.026	1.197 0.002	1.078 0.016	1.028 0.008	1.261 0.002
1.170 -0.014	1.245 -0.014	1.150 0.007	1.027 0.007	1.083 0.012	0.863 0.016	1.307 0.005	1.089 0.002
1.115 -0.011	0.816 0.018	1.150 0.006	1.227 0.010	1.028 0.003	1.301 0.009	0.853 0.018	1.116 0.000
0.904 0.011	0.912 0.003	1.280 0.001	1.080 0.009	1.261 -0.010	1.089 -0.001	1.116 0.007	0.765 0.011

0.722 -0.025
0.878 -0.009

Figure 16

CALCULATED AND MEASURED POWER DISTRIBUTIONS AT BOC 4
(IMPROVED METHODS)

MEAS C-M							
						0.681 −0.019	0.876 −0.015
			0.724 −0.012	0.986 −0.004	1.115 0.003	1.102 −0.014	1.065 −0.005
		0.835 −0.024	1.207 −0.007	1.201 0.004	1.011 0.005	0.895 −0.005	1.242 −0.015
	0.839 −0.026	1.233 −0.023	1.101 −0.012	1.036 0.000	1.226 0.018	0.938 −0.007	0.967 −0.005
0.721 −0.006	1.213 −0.008	1.102 −0.009	1.043 0.003	0.994 0.008	0.923 0.008	1.000 0.009	0.878 0.002
0.995 −0.007	1.216 −0.004	1.045 0.005	1.000 0.012	0.939 0.025	1.099 0.013	0.829 0.012	1.059 −0.002
1.130 −0.005	1.023 0.002	1.245 0.014	0.929 0.012	1.099 0.020	0.852 0.016	1.082 0.011	0.846 0.009
1.109 −0.013	0.899 0.003	0.944 0.010	1.003 0.015	0.826 0.019	1.081 0.013	0.989 0.006	1.102 −0.014
1.065 0.004	1.242 0.001	0.967 0.010	0.878 0.011	1.059 0.003	0.846 0.009	1.102 −0.016	0.708 −0.021

0.691 −0.024
0.880 −0.013